

Type I IFN blockade uncouples immunotherapy-induced antitumor immunity and autoimmune toxicity

Scott R. Walsh,¹ Donald Bastin,¹ Lan Chen,¹ Andrew Nguyen,¹ Christopher J. Storbeck,^{2,3} Charles Lefebvre,⁴ David Stojdl,^{3,4} Jonathan L. Bramson,¹ John C. Bell,^{2,3} and Yonghong Wan¹

¹McMaster Immunology Research Centre, Department of Pathology and Molecular Medicine, McMaster University, Hamilton, Ontario, Canada. ²Centre for Innovative Cancer Research, Ottawa Hospital Research Institute, Ottawa, Ontario, Canada. ³Department of Biochemistry, Microbiology and Immunology, University of Ottawa, Ottawa, Ontario, Canada. ⁴Children's Hospital of Eastern Ontario Research Institute, Ottawa, Ontario, Canada.

Despite its success in treating melanoma and hematological malignancies, adoptive cell therapy (ACT) has had only limited effects in solid tumors. This is due in part to a lack of specific antigen targets, poor trafficking and infiltration, and immunosuppression in the tumor microenvironment. In this study, we combined ACT with oncolytic virus vaccines (OVVs) to drive expansion and tumor infiltration of transferred antigen-specific T cells and demonstrated that the combination is highly potent for the eradication of established solid tumors. Consistent with other successful immunotherapies, this approach elicited severe autoimmune consequences when the antigen targeted was a self-protein. However, modulation of IFN- α / β signaling, either by functional blockade or rational selection of an OVV backbone, ameliorated autoimmune side effects without compromising antitumor efficacy. Our study uncovers a pathogenic role for IFN- α / β in facilitating autoimmune toxicity during cancer immunotherapy and presents a safe and powerful combinatorial regimen with immediate translational applications.

Introduction

Immunotherapy has become a powerful therapeutic paradigm in cancer treatment. CD8⁺ T cells play a prominent role in tumor clearance, given their ability to selectively recognize tumor antigens and directly kill tumor cells. Typically, antigens targeted by CD8⁺ T cells can be broadly separated into 2 categories: non-self antigens and self-antigens. Non-self antigens are derived from either mutated cancer cell genes (neoantigens) or viral products, while tumor-associated self-antigens are cellular genes that are overexpressed in tumors, including cancer-testis antigens and tissue differentiation antigens. Neoantigens and viral antigens tend to be more immunogenic than self-antigens and thus represent desirable targets for CD8⁺ T cell-based immunotherapies (1). However, these antigens are not readily identifiable, and the vast majority of tumors do not harbor a high mutational load or detectable oncovirus gene expression (2, 3). Consequently, cancer targeting will probably continue to rely on the recognition of tumor-associated self-antigens, which have been extensively explored as targets for both vaccines and adoptive cell therapies (ACTs) (4–6).

Self-tumor antigens are derived from germline-encoded proteins, thus, targeting these antigens poses an inherent risk of autoimmune consequence. Some preclinical studies have shown

that antitumor immunity can be generated without autoimmune side effects, suggesting that there is a therapeutic window due to enhanced expression of target antigens on tumor cells (7, 8). However, other studies have indicated that this threshold can be readily exceeded when therapeutic intensity is heightened, arguing that autoimmune pathology may be an unavoidable consequence of effective immunotherapy (9–11). Indeed, the remarkable benefits of cancer immunotherapies observed in clinical trials, most notably checkpoint blockade and ACTs, are often paralleled by robust autoimmune adverse effects (12, 13). Nonetheless, it is still not well understood how autoreactive T cells can discriminate between tumor tissues and normal tissues or how they are regulated in both settings.

Traditional ACT protocols exploit the antigen-specific cytolytic potential of CD8⁺ T cells by transferring terminally differentiated effector T (T_{EFF}) cells, but more recent evidence has shown that less differentiated cells, such as central memory T (T_{CM}) cells, show superior performance (14, 15). Therefore, in this study, we used an immunotherapy platform that combines adoptive transfer of tumor-reactive T_{CM} cells with oncolytic virus vaccines (OVVs). Combinatorial use of T_{CM} cell ACT and OVVs produced high-intensity systemic antitumor immune responses via rapid expansion of transferred T cells and robust regression of established tumors in the absence of host conditioning or exogenous IL-2. Here, we explored the molecular signals regulating the development of autoimmunity following combined ACT and OVVs. We demonstrate that induction of IFN- α and IFN- β expression during combined ACT and OVV therapy led to undesirable autoimmune destruction. Further analyses indicated that systemic IFN- α / β upregulated MHC class I (MHC

Conflict of interest: SRW, LC, and YW are inventors on a patent submitted by McMaster University that covers the use of adoptive T cell therapy and oncolytic virus vaccination combination therapy (international application no. PCT/CA2017/050772; World Intellectual Property Organization [WIPO] publication no. WO/2017/219150).

License: Copyright 2019, American Society for Clinical Investigation.

Submitted: March 9, 2018; **Accepted:** November 6, 2018.

Reference information: *J Clin Invest.* 2019;129(2):518–530.

<https://doi.org/10.1172/JCI121004>.

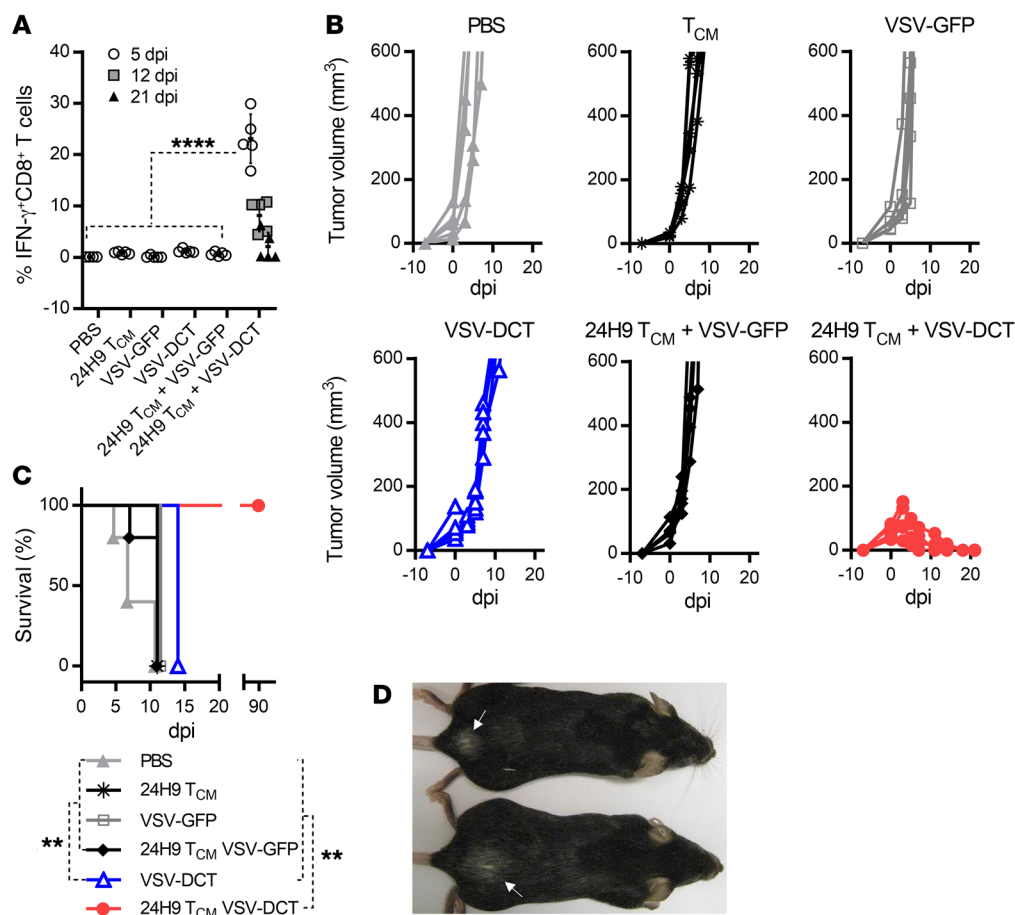


Figure 1. Combination T_{CM} cell ACT plus OVV targeting DCT induces complete tumor regression coupled with localized vitiligo. (A) DCT-specific CD8⁺ T cell responses were evaluated in B16F10 tumor-bearing C57BL/6 mice at the designated time point after administration of the indicated treatment, with 0 dpi representing the day of OVV injection and results expressed as the percentage of CD8⁺ T cells in the peripheral circulation that produced IFN- γ upon stimulation with the immunodominant DCT peptide. (B) Tumor volume (mm³) was assessed on the indicated post-infection days. (C) Survival of the treated mice. (D) Representative image of vitiligo (indicated by white arrows) on the backs of 2 of the treated mice. Data for A–C are representative of 2 independent experiments ($n = 5$ per group) and are shown as the mean \pm SD. ** $P < 0.01$ and *** $P < 0.0001$, by 1-way ANOVA with Holm-Sidak correction for multiple comparisons (A) and log-rank (Mantel-Cox) test (C).

l) expression on the target organ, rendering it susceptible to destruction by transferred autoreactive CD8⁺ T cells. Strikingly, blocking IFN- α and IFN- β signaling completely abrogated the autoimmune side effect, without compromising antitumor efficacy, revealing the IFN- α /- β pathway as a druggable target for the suppression of immunotherapy-induced autoimmune sequelae. Separation of anticancer immunity and the associated deleterious autoimmunity could be achieved by the rational selection of an OVV backbone with inherent IFN- α /- β -blocking activity, offering a powerful combinatorial regimen with immediate translational implications.

Results

Targeting a melanocyte differentiation antigen by ACT plus a vesicular stomatitis virus-based oncolytic vaccine leads to both tumor regression and vitiligo development. Our preclinical studies have demonstrated that vesicular stomatitis virus-based (VSV-based) vaccine vectors are highly potent at boosting memory T cell expansion (6, 16). Thus, to evaluate the combination platform of ACT and an OVV, we chose to use VSV as an OVV backbone with engineered expression of dopachrome tautomerase (DCT), a melanocyte differentiation antigen that is often overexpressed by melanoma cells. 24H9 mice, a transgenic mouse strain that expresses a T cell receptor (TCR) specific for the immunodominant peptide of DCT, were used as a source for the generation of DCT-specific CD8⁺ T_{CM} cells (17) (Supplemental Figure 1A; supplemental

material available online with this article; <https://doi.org/10.1172/JCI121004DS1>). C57BL/6 mice were engrafted with 10⁵ B16F10 cells via intradermal injection and treated 6 days later by i.v. infusion with 3 \times 10⁶ 24H9 T_{CM} cells, 1 \times 10⁹ PFU VSV-DCT, or both at a 24-hour interval (Supplemental Figure 1B). Mice were also treated with VSV-GFP (a VSV vector encoding GFP in place of the antigen transgene) alone and in combination with T_{CM} cells as a control.

We detected only a nominal DCT-specific CD8⁺ T cell response in mice treated with T_{CM} cells, VSV-GFP, VSV-DCT, or 24H9 T_{CM} cells plus VSV-GFP (Figure 1A), which was not significantly different from the response seen in PBS-treated mice, and none of these therapies had a significant impact on tumor growth or survival (Figure 1, B and C). Combination of the 2 therapeutic components elicited a robust DCT-specific T cell response that peaked at 5 days post infection (dpi), with approximately 23% of circulating CD8⁺ T cells in these mice responding to DCT peptide stimulation (Figure 1A). Consistent with T cell responses, complete and durable tumor regression as well as significantly prolonged survival were achieved in mice that received combination therapy, confirming its potency (Figure 1, B and C). All surviving mice developed vitiligo, an indication of melanocyte damage, indicating a link between combination therapy-induced antitumor immunity and autoimmunity when the target antigen was a self-protein (Figure 1D). However, such a mild consequence in a nonvital organ is clinically manageable or even tolerable and does not represent a significant clinical concern.

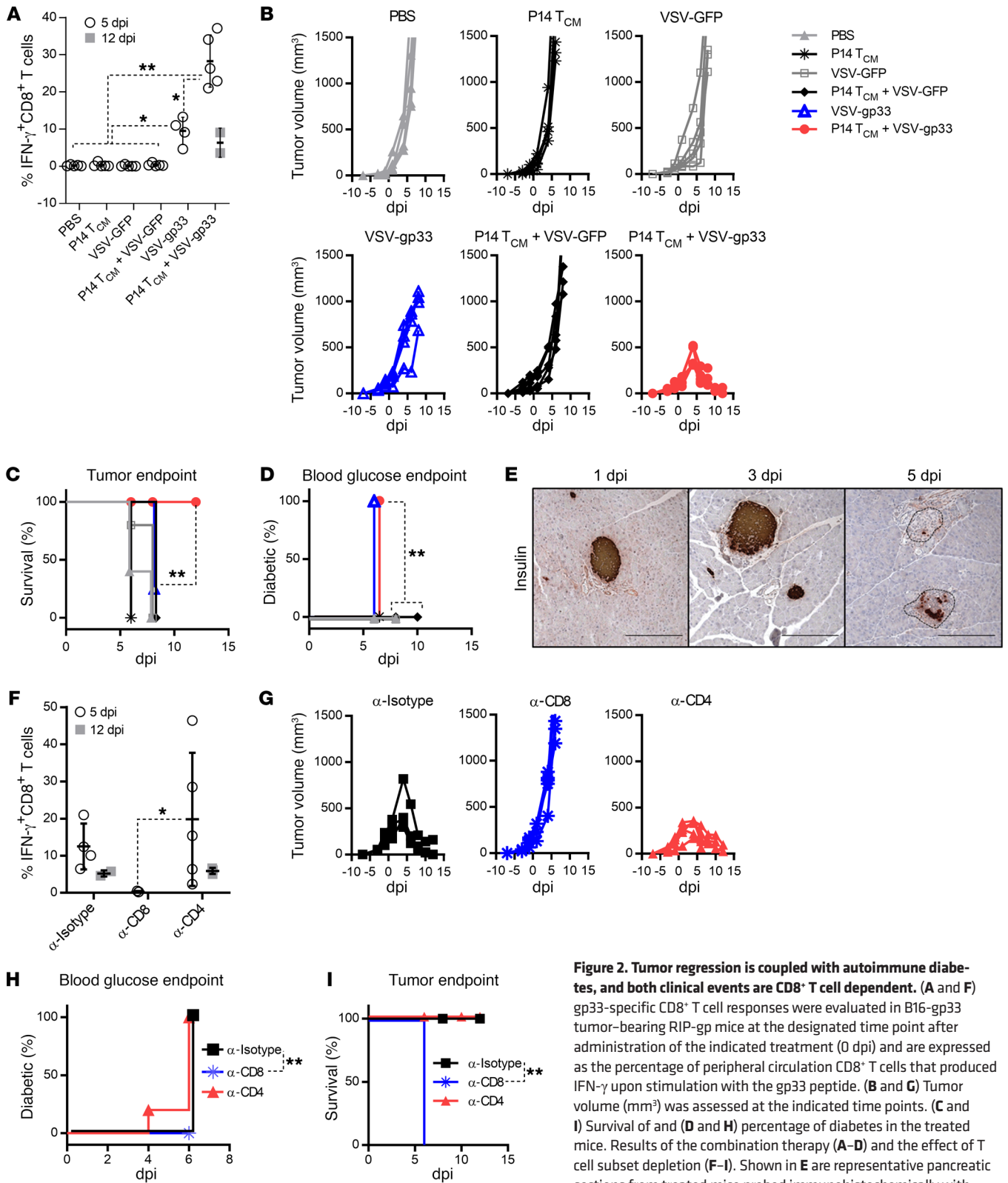


Figure 2. Tumor regression is coupled with autoimmune diabetes, and both clinical events are CD8⁺ T cell dependent. (A and F) gp33-specific CD8⁺ T cell responses were evaluated in B16-gp33 tumor-bearing RIP-gp mice at the designated time point after administration of the indicated treatment (0 dpi) and are expressed as the percentage of peripheral circulation CD8⁺ T cells that produced IFN- γ upon stimulation with the gp33 peptide. (B and G) Tumor volume (mm³) was assessed at the indicated time points. (C and I) Survival of and (D and H) percentage of diabetes in the treated mice. Results of the combination therapy (A–D) and the effect of T cell subset depletion (F–I). Shown in E are representative pancreatic sections from treated mice probed immunohistochemically with an anti-insulin mAb. Scale bars: 20 μ m. Data for A–C represent 1 of 3 experiments; $n = 4$ per group (VSV-gp33) and $n = 5$ per group (PBS, P14T_{CM} cells, VSV-GFP, P14T_{CM} cells plus VSV-GFP). Data for F–I are representative of 2 independent experiments; $n = 5$ per group (anti-CD8 [α -CD8] and anti-CD4 [α -CD4]) and $n = 4$ per group (anti-isotype [α -Isotype]). * $P < 0.05$ and *** $P < 0.01$, by 1-way ANOVA with Holm-Sidak correction for multiple comparisons (A and F) and log-rank (Mantel-Cox) test (C, D, H, and I).

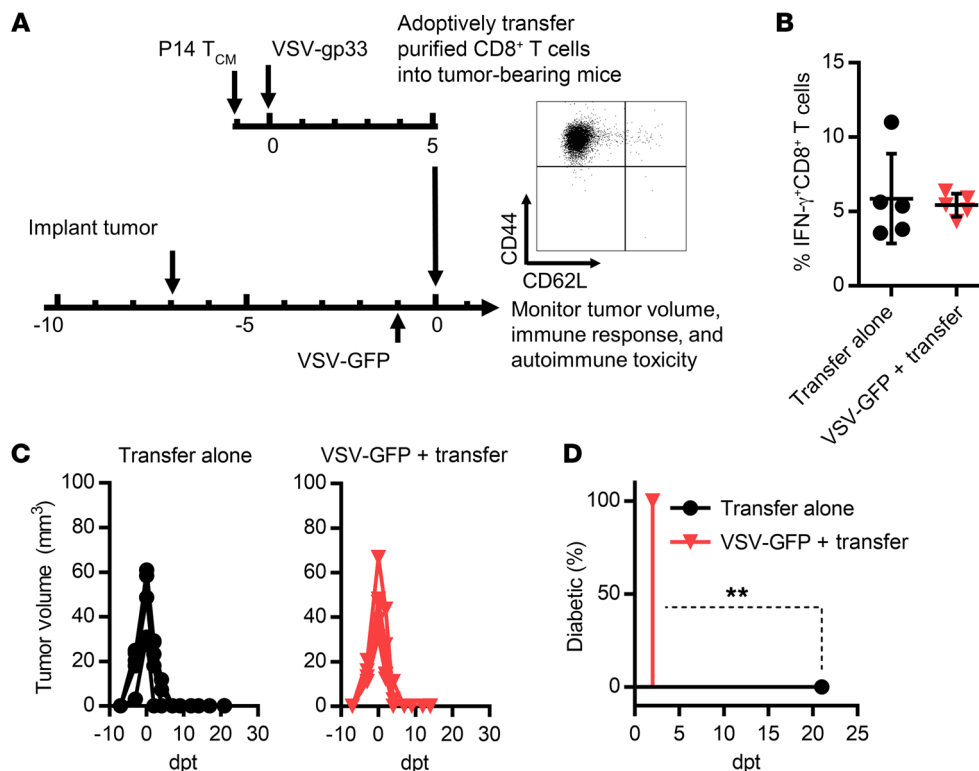


Figure 3. VSV-induced inflammation is required for diabetes and features excessive systemic IFN- α / β levels. (A) Schematic representation of the experimental protocol and phenotypic analysis of gp33-tetramer-positive CD8⁺ T cells in the transferred cell population. (B) The quantity of gp33-specific CD8⁺ T cells in the circulation 1 day after T cell infusion into B16-gp33 tumor-bearing RIP-gp mice was determined by IFN- γ staining. Tumor volume (C) and diabetes development (D) were assessed on the indicated days post transfer (dpt) (** $P = 0.0027$). Data for B–D represent 1 of 3 experiments ($n = 5$ per group) and are shown as the mean \pm SD. Data were analyzed using a 2-tailed Student's t test (B) and a log-rank (Mantel-Cox) test (D).

Tumor regression induced by ACT plus VSV is coupled with severe diabetes when the target antigen is expressed in pancreatic β islet cells. To explore autoimmune sequelae produced by ACT plus OVV in a second model in which the shared target antigen was expressed on a vital organ, we extended our analysis to the RIP-gp mouse model, in which therapy-induced autoimmune toxicity would result in pancreatic β cell destruction and diabetes. For these studies, we used the B16-gp33 tumor, which is a derivative of the B16 melanoma cell line modified to constitutively express gp33, the immunodominant peptide from the lymphocytic choriomeningitis virus (LCMV) glycoprotein (18). B16-gp33 tumors were implanted into RIP-gp-transgenic mice, which express gp33 specifically on pancreatic β cells (19). In this model, gp33 serves as a surrogate self-antigen that permits the monitoring of immune attack against both the tumor and pancreatic β cells. RIP-gp mice bearing intradermal B16-gp33 tumors were treated with T_{CM} cells derived from gp33-specific P14 TCR-transgenic T cells, followed by VSV-gp33 vaccination. Similar to the observations made in the DCT model, VSV-gp33 induced a robust expansion of P14 T_{CM} cells that peaked on day 5 after vaccination, and complete tumor regression was achieved within 12 days, resulting in significantly prolonged survival with respect to the tumor endpoint (Figure 2, A–C). Coincident with the peak of P14 T cell responses, the treated mice became diabetic by day 5 (Figure 2D) as a result of loss of insulin-producing β cells in the pancreatic islets (Figure 2E). P14 T_{CM} cells, VSV-GFP alone, and P14 T_{CM} cells plus VSV-GFP were not able to induce an antigen-specific response

significantly higher than that achieved with PBS treatment and had no impact on either tumor growth or diabetes development, confirming that autoreactive T cells or systemic inflammatory responses alone are insufficient to mediate the destruction of antigen-positive tumor cells or normal cells (Figure 2, A–D). Interestingly, we observed that VSV-gp33 alone (but not VSV-GFP) was able to elicit diabetes (Figure 2D), probably as a result of the boosting of tumor-primed endogenous gp33-specific T cells. However, the magnitude and kinetics of endogenous T cell expansion were insufficient to control tumor outgrowth and significantly prolong survival (Figure 2, A–C), reinforcing the necessity of ACT for a maximum antitumor effect in the combination therapy platform.

We next performed *in vivo* depletion of lymphocyte subsets during combination therapy to characterize the T cell subsets required for antitumor and anti- β cell activity (Supplemental Figure 1C). Selective depletion of CD8⁺ T cells crippled the gp33-specific response and eliminated both tumor regression and diabetes (Figure 2, F–I). In contrast, we found that depletion of CD4⁺ T cells did not significantly block tumor regression or diabetes induction (Figure 2, F–I), confirming that CD8⁺ T cells are the primary effector component mediating both tumor regression and β cell destruction.

Autoimmune diabetes is associated with excessive production of IFN- α / β . VSV infection is known to induce an acute proinflammatory reaction, so we speculated that the VSV-induced inflammatory profile might modulate pancreatic β cell damage by autoreactive T cells. To address this question, bulk purified CD8⁺ T cells

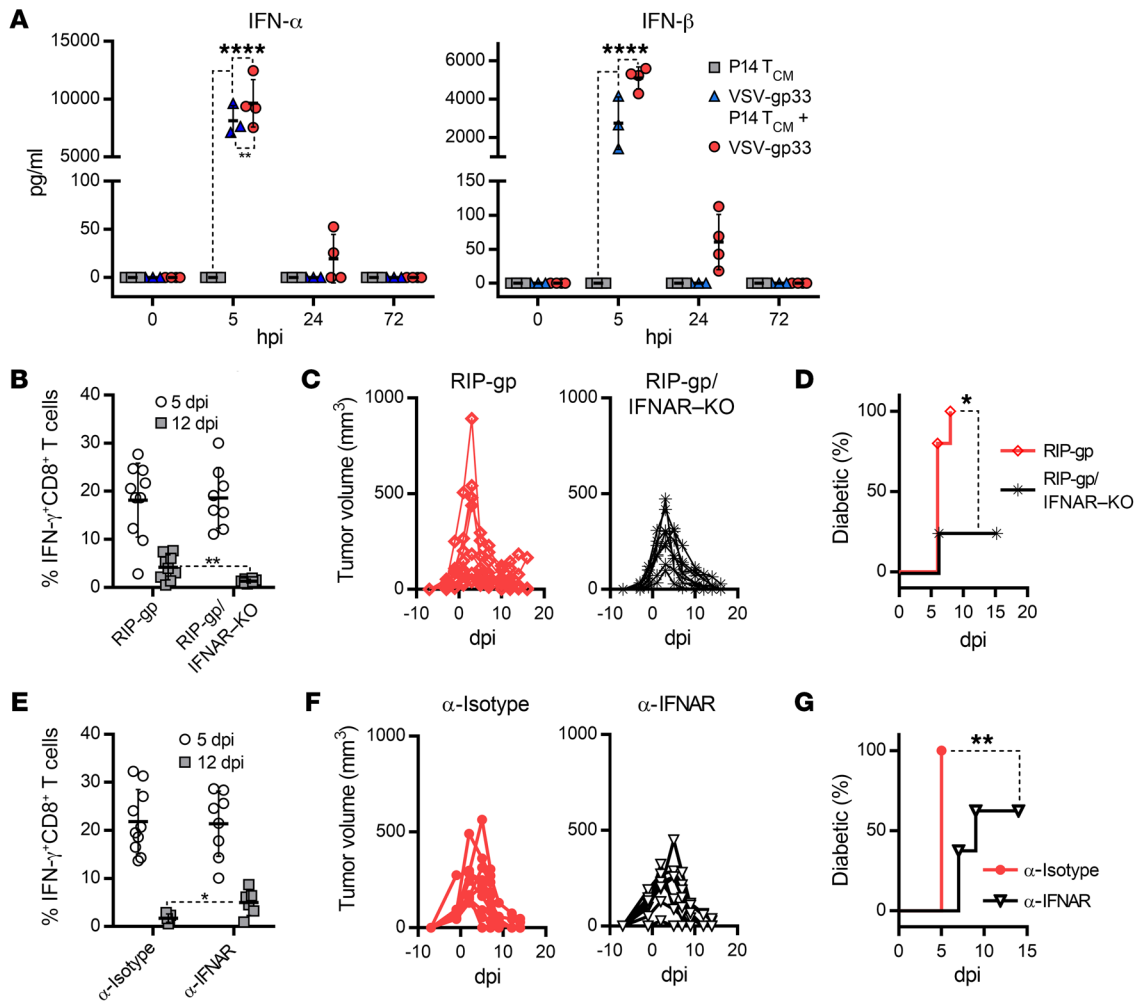


Figure 4. IFN- α /- β signaling couples diabetes with tumor regression. (A) Systemic levels of IFN- α and IFN- β induced by the combination therapy and each component when used alone, assayed in plasma from treated B16-gp33 tumor-bearing RIP-gp mice ($n = 4$). (B and E) gp33-specific CD8 $^+$ T cell responses, (C and F) tumor volume, and (D and G) percentage of mice with diabetes induced by the combination therapy were measured on the indicated dpi. (B–D) $n = 10$ RIP-gp mice and $n = 8$ RIP-gp/IFNAR-KO mice; (E–G) $n = 10$ anti-isotype Ab-treated RIP-gp mice and $n = 8$ anti-IFNAR Ab-treated RIP-gp mice. Data for B–G represent 1 of 3 experiments and are shown as the mean \pm SD. * $P < 0.05$, ** $P < 0.01$, and **** $P < 0.0001$, by 1-way ANOVA with Holm-Sidak correction for multiple comparisons (A), 2-tailed Student's t test (B and E), and log-rank (Mantel-Cox) test (D and G).

from splenocytes of mice treated with the combination protocol were transferred into B16-gp33 tumor-bearing RIP-gp mice (Figure 3A). Transferred gp33-specific CD8 $^+$ T cells had an effector phenotype (CD44 $^+$ CD62L $^-$) (Figure 3A) and could subsequently be detected in the circulation of recipient mice (~6%) (Figure 3B). We observed tumor regression after transfer in the absence of diabetes (Figure 3, C and D), confirming that inflammation was the determining factor for autoimmune consequences following combination therapy. This conclusion was further supported by the fact that treatment with VSV-GFP prior to T cell transfer recoupled diabetes with tumor regression (Figure 3, B–D).

We measured a panel of pro- and antiinflammatory cytokines from the plasma of mice that had received combination therapy. Within 5 hours of VSV infection, we observed a massive induction of IFN- α and IFN- β cytokines that tapered off after 24 hours (Figure 4A). Although we detected significant changes in the levels of the other cytokines assayed, these changes were not nearly as drastic or significant as those for IFN- α /- β (Supplemental Figure

2). To determine the role of IFN- α /- β in tumor regression and diabetes induction concurrently, we crossbred RIP-gp mice with mice lacking the IFNAR1 gene. The resultant mice (termed RIP-gp/IFNAR-KO mice) maintained LCMV-gp protein expression in pancreatic β cells but lacked the IFN- α /- β receptor, rendering the β cells incapable of sensing IFN- α /- β signaling. Tumor-bearing RIP-gp/IFNAR-KO mice and their WT RIP-gp counterparts were treated with P14 T $_{CM}$ cells and Δ G-VSV-gp33, a replication-deficient VSV vector (lacking the viral glycoprotein gene) that is tolerated by IFNAR-KO mice. Figure 4, B and C, shows that the magnitude of gp33-specific CD8 $^+$ T cell responses and the kinetics of tumor regression were equivalent in RIP-gp/IFNAR-KO and WT RIP-gp mice but that the incidence of diabetes was severely abrogated in the RIP-gp/IFNAR-KO mice (Figure 4D). To ensure that this phenomenon was not unique to the IFNAR-KO background, we treated RIP-gp mice with an IFNAR1-specific Ab to functionally block interaction of IFN- α /- β with its receptor. As shown in Figure 4, E and F, the magnitude of gp33-specific CD8 $^+$ T cell responses

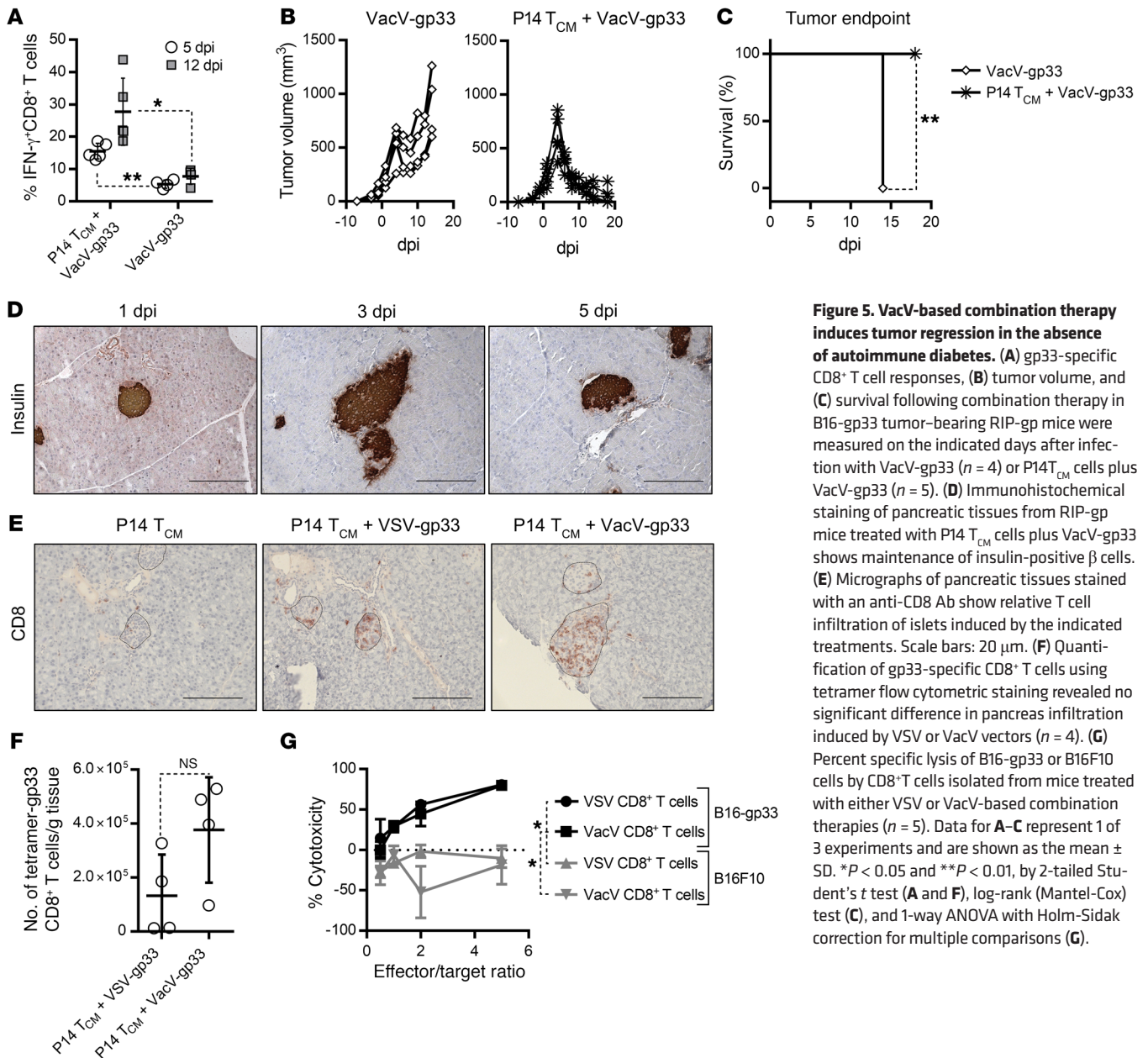


Figure 5. VacV-based combination therapy induces tumor regression in the absence of autoimmune diabetes. (A) gp33-specific CD8⁺ T cell responses, (B) tumor volume, and (C) survival following combination therapy in B16-gp33 tumor-bearing RIP-gp mice were measured on the indicated days after infection with VacV-gp33 (*n* = 4) or P14T_{CM} cells plus VacV-gp33 (*n* = 5). (D) Immunohistochemical staining of pancreatic tissues from RIP-gp mice treated with P14 T_{CM} cells plus VacV-gp33 shows maintenance of insulin-positive β cells. (E) Micrographs of pancreatic tissues stained with an anti-CD8 Ab show relative T cell infiltration of islets induced by the indicated treatments. Scale bars: 20 μ m. (F) Quantification of gp33-specific CD8⁺ T cells using tetramer flow cytometric staining revealed no significant difference in pancreas infiltration induced by VSV or VacV vectors (*n* = 4). (G) Percent specific lysis of B16-gp33 or B16F10 cells by CD8⁺ T cells isolated from mice treated with either VSV or VacV-based combination therapies (*n* = 5). Data for A–C represent 1 of 3 experiments and are shown as the mean \pm SD. **P* < 0.05 and ***P* < 0.01, by 2-tailed Student’s *t* test (A and F), log-rank (Mantel-Cox) test (C), and 1-way ANOVA with Holm-Sidak correction for multiple comparisons (G).

and the kinetics of tumor regression were not affected by anti-IFNAR Ab blockage, but the incidence of diabetes was significantly decreased in the anti-IFNAR-treated mice (62.5%) compared with the anti-isotype-treated mice (100%) (Figure 4G). Also, in those mice that developed diabetes, its onset was significantly delayed in the anti-IFNAR-treated group (median of disease onset at 9 dpi) compared with the anti-isotype-treated group (median of disease onset at 5 dpi). It is worth noting that the effect of IFNAR blockade was not as pervasive as that of IFNAR-KO, but this was likely the result of residual IFN- α / β signaling in the context of IFNAR Ab blockade compared with the absolute lack of IFN- α / β signaling in IFNAR-KO mice. Finally, we also depleted plasmacytoid DCs (pDCs), the main source of IFN- α / β released during VSV infection (20), before administering the combination therapy, and again observed a delay or decrease in diabetes incidence,

despite the negligible effect on the magnitude of the gp33-specific response and tumor regression (Supplemental Figure 3, A–C). Together, these data indicate that sensing of IFN- α / β by pancreatic β cells is a requisite component of diabetes development but is dispensable for the antitumor effect of the same response.

Vaccinia virus completely separates antitumor immunity from autoimmune diabetes. An important feature of our therapeutic strategy is that we can change the OVV backbone in order to take advantage of the biological properties of different viral vectors. Having established a pathogenic role of excessive IFN- α / β induced by VSV, we hypothesized that vaccinia virus (VacV) might mitigate undesired autoimmune side effects, given its intrinsic ability to both suppress IFN- α / β production and scavenge secreted IFN- α / β through expression of the B18R protein (21). To test this hypothesis, we first replaced VSV with VacV as an alternative

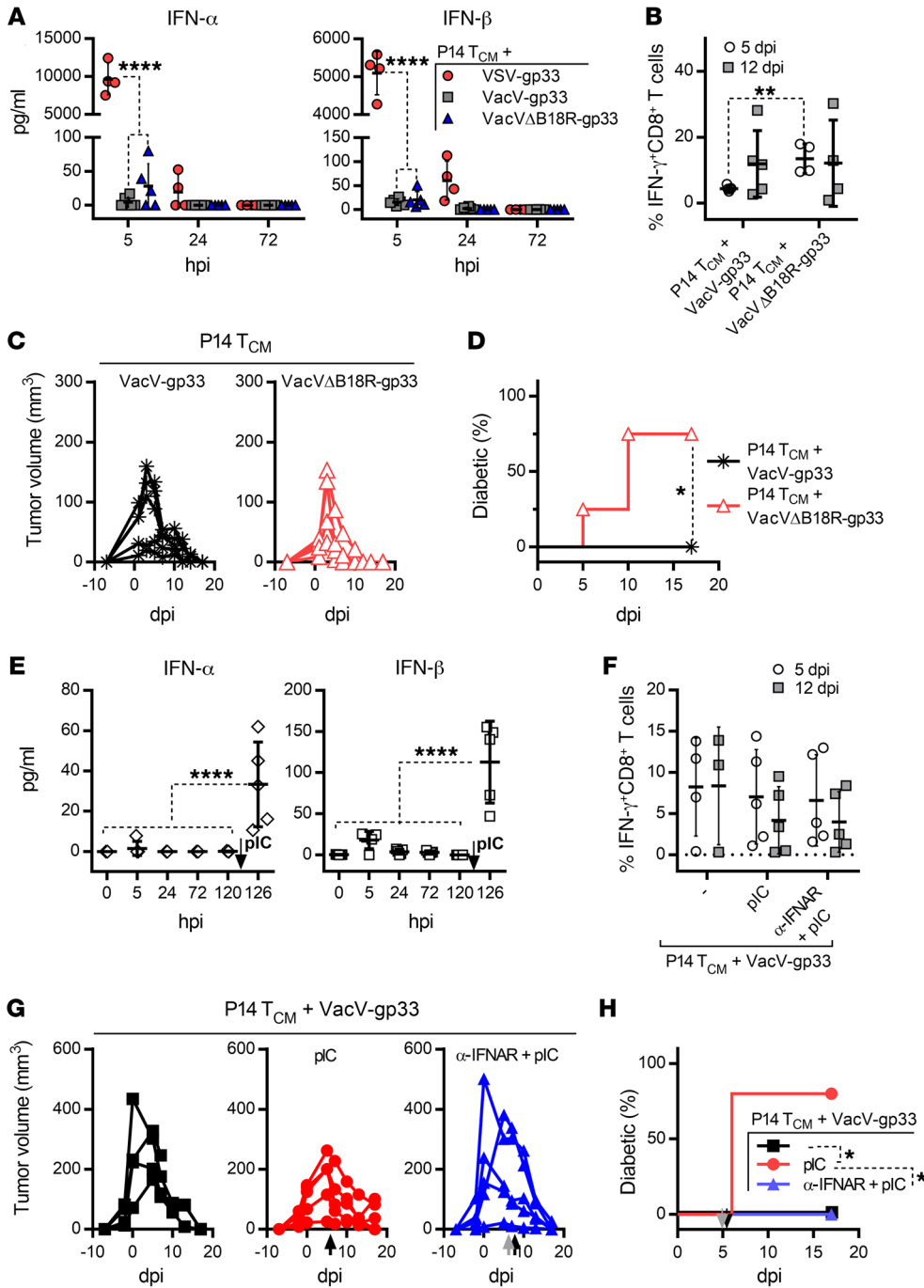


Figure 6. B18R-mediated neutralization of IFN- α / β decouples tumor regression from autoimmune diabetes but can be overwhelmed by pIC treatment. (A) Systemic levels of IFN- α and IFN- β detected in plasma samples taken from B16-gp33 tumor-bearing RIP-gp mice at the indicated time point (hours post infection [hpi]) after injection of the VSV-gp33 ($n = 4$), VacV-gp33 ($n = 6$), or Vac Δ B18R-gp33 ($n = 5$) component of the combination therapy. (B) gp33-specific CD8 $^+$ T cell responses and (C) tumor volume were measured on the indicated dpi in B16-gp33 tumor-bearing RIP-gp mice treated with P14 T $_{CM}$ cells plus VacV-gp33 ($n = 5$) or P14 T $_{CM}$ cells plus Vac Δ B18R-gp33 ($n = 4$). (D) Percentage of mice that developed diabetes. (E) Systemic levels of IFN- α and IFN- β in plasma samples ($n = 5$), (F) gp33-specific CD8 $^+$ T cell responses, and (G) tumor volume induced by the combination therapy were measured on the indicated day following infection with VacV-gp33 ($n = 4$). This was followed by pIC treatment on day 5 after infection (120 hpi), as shown by the black arrows in E, G and H ($n = 5$). An additional group received a bolus of the IFNAR-blocking Ab 2 hours prior to pIC treatment, as shown by the gray arrow in G and H ($n = 5$). (H) Percentage of mice that developed diabetes. Data for B–D and F–H are representative of 2 independent experiments and are shown as the mean \pm SD. * $P < 0.05$, ** $P < 0.01$, and **** $P < 0.0001$, by 2-way ANOVA (A and F) or 1-way ANOVA (E) with Holm-Sidak correction for multiple comparisons, 2-tailed Student’s t test (B), and log-rank (Mantel-Cox) test (D and H).

oncolytic boost vector in the context of combination with P14 T $_{CM}$ cells. As shown in Figure 5, A and B, VacV-gp33 was able to generate a robust systemic response with a similar peak of the gp33-specific CD8 $^+$ T cell response (~30%), tumor regression kinetics, and significantly prolonged survival, as was previously seen with the VSV-based therapy (Figure 2, A and B). Consistent with our hypothesis, VacV-stimulated tumor regression occurred in the complete absence of autoimmune diabetes (Figure 5C). Histological staining of pancreatic tissue from mice treated with VacV confirmed the maintenance of insulin-positive β cells throughout the course of the therapy (Figure 5D). Additionally, when given alone, VacV-gp33 only induced a modest response (Figure 5A) and

was unable to control the tumor or significantly prolong survival (Figure 5, B and C), further highlighting the need to use ACT and OVVs in combination.

Figure 5E shows a similar infiltration of pancreatic islets with CD8 $^+$ T cells following VacV and VSV-based combination treatment, which was probably a result of the large systemic response induced by these therapies, especially considering the limited infiltration observed with P14 T $_{CM}$ cell monotherapy. Indeed, quantification with a gp33 tetramer confirmed that the number of gp33-specific T cells in the pancreas after either virus treatment was not significantly different (Figure 5F), suggesting that VacV and VSV do not differ in their ability to affect pancreatic infil-

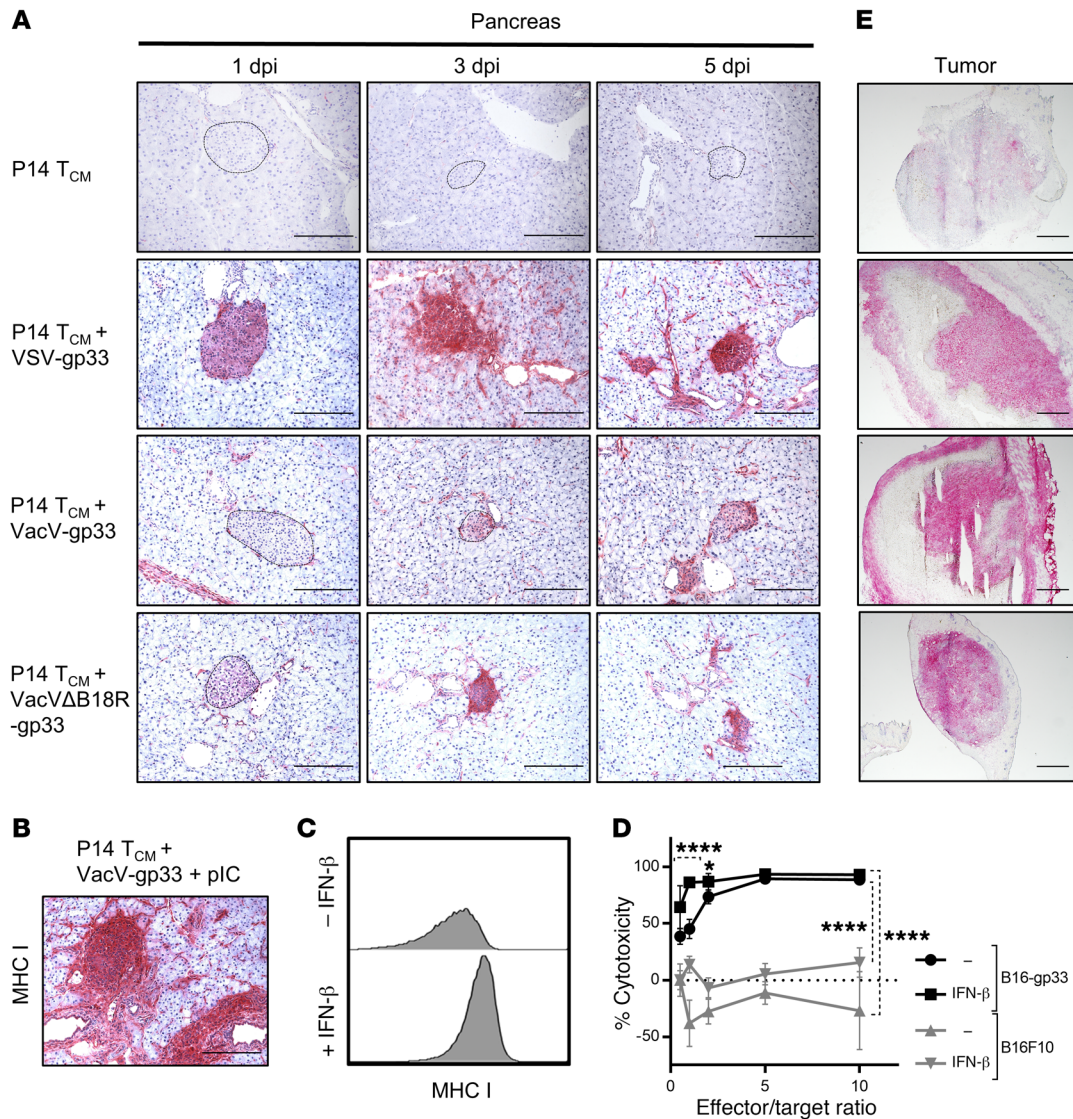


Figure 7. IFN- α - β -induced upregulation of MHC I enhances antigen-specific cytotoxicity, resulting in autoimmune diabetes. (A) Immunohistochemical staining of pancreatic tissues from treated RIP-gp mice showed increased MHC I expression on islets after VSV-gp33 and Vac Δ B18R-gp33 treatment but only low MHC I expression levels on islet cells after treatment with VacV-gp33-based combination therapy. (B) Pancreatic islets showed intense MHC I staining upon i.p. injection with pIC on day 5 after treatment with the VacV-based combination therapy. Scale bar: 20 μ m. (C) Flow cytometric evaluation of B16-gp33 cells treated in vitro with IFN- β showed upregulation of MHC I expression. (D) Combination therapy-generated cytotoxicity of CD8⁺ T cells on B16-gp33 cells but not gp33-negative B16F10 cells after pretreatment with IFN- β ($n = 10$). * $P < 0.05$ and **** $P < 0.0001$ by 2-way ANOVA with Holm-Sidak correction for multiple comparisons. (E) Tumor tissues from treated mice showed similar MHC I expression profiles when probed immunohistochemically, regardless of the viral vector used. Scale bars: 50 μ m.

tration of expanded CD8⁺ T cells. Furthermore, in vitro analysis indicated that CD8⁺ T cells generated by the VacV protocol were equally capable of killing target cells compared with those generated by VSV (Figure 5G), confirming that the CD8⁺ T cells were functionally equivalent in both cases.

We next measured the kinetics of cytokine production in the blood and confirmed that VacV only induced a minimum level of IFN- α - β compared with VSV vaccination (Figure 6A). Furthermore, to elucidate the role of B18R inhibition in determining the autoimmune outcome of the therapy, we generated a recombinant VacV-gp33 lacking an intact B18R coding region (Vac Δ B18R-gp33). We found that Vac Δ B18R-gp33 treatment induced higher levels of IFN- α - β than VacV-gp33 treatment, although statistical

significance was not reached (Figure 6A). Deletion of B18R did not alter the peak magnitude of the gp33-specific CD8⁺ T cell response at 12 dpi or the tumor regression kinetics, but the majority of mice treated with B18R-deleted virus developed diabetes (Figure 6, B–D). In addition, to overwhelm B18R inhibition, we delivered Poly (I:C) (pIC) 5 days after VacV vaccination, correlating with the time point at which the therapy-induced T cells reached the pancreas. Treatment with pIC induced a significant increase in IFN- α - β levels, which had no significant effect on the magnitude of gp33-specific CD8⁺ T cell responses or tumor regression (Figure 6, E–G), but diabetes was induced in all of the treated mice (Figure 6H). Pretreatment with the IFNAR-blocking Ab before pIC completely prevented diabetes, with no significant effect on the

gp33-specific response or tumor regression (Figure 6, E-H). These results reinforce the idea of a critical role of IFN- α /- β in mediating post-therapy autoimmune sequelae, which can be avoided by rational selection of an OVV vector.

Autoimmune diabetes is associated with IFN- α /- β -mediated upregulation of MHC I on β cells. An increase in MHC I expression levels on tumor and normal cells resulting in increased susceptibility to antigen-specific CD8⁺ T cell attack has previously been shown to share a correlative relationship with systemic induction of IFN- α /- β (22–24). Therefore, we hypothesized that VSV-induced IFN- α /- β may have upregulated MHC I levels on the surface of β cells and rendered them more susceptible to immune attack by the infiltrating P14 T cells. Immunohistochemical probing of pancreatic tissues from combination therapy-treated mice showed a dramatic upregulation of MHC I expression on β cells following VSV vaccination compared with the low expression level seen after T_{CM} cell transfer alone (Figure 7A). MHC I levels were highest 5 days after vaccination, coinciding with the onset of diabetes (Figure 2C).

Histological analysis revealed a correlation between the treatment of islets with VacV, which showed low level MHC I expression, and the deletion of B18R, which showed high level MHC I expression, supporting our hypothesis that inhibition of IFN- α /- β -mediated MHC I upregulation by B18R prevents the recognition of pancreatic β cells by infiltrating autoreactive T cells (Figure 7A). We performed 2 more experiments to confirm this correlation. First, staining of pancreatic tissues from mice treated with pIC following VacV-based combination therapy revealed enhanced levels of MHC I compared with VacV treatment alone and levels similar to those detected with VSV treatment (Figure 7B). Second, treatment of B16-gp33 cells with IFN- β in vitro dramatically increased MHC I expression (Figure 7C) and enhanced their killing by purified gp33-specific CD8⁺ T cells from mice treated with the combination therapy (Figure 7D), a phenomenon that is likely shared by pancreatic β cells.

Interestingly, in contrast to pancreatic islets, we observed intense MHC I staining throughout the tumor (Figure 7E), irrespective of which OVV treatment was administered, demonstrating that IFN- α /- β is not required for the upregulation of MHC I on tumor cells when an oncolytic virus (OV) is used. It is likely that local inflammatory effects of OV replication in the tumor induced other inflammatory signals that could maintain or enhance MHC I expression on tumor cells independently of IFN- α /- β (25, 26).

Discussion

In this study, we characterized the robust antitumor effect of an immunotherapeutic protocol that combines adoptive transfer of tumor-specific T_{CM} cells with an oncolytic vaccine. The approach allows the rapid expansion of adoptively transferred T_{CM} cells and effective tumor infiltration to eradicate well-established solid tumors. This combination platform has broad clinical implications, given its potency and flexibility for targeting different tumor antigens and/or incorporating different OVV backbones. Most important, using this approach, we have identified a pathogenic role for IFN- α /- β in mediating autoimmune toxicity as a consequence of cancer immunotherapy and offer a practical solution to block or minimize IFN- α /- β signaling, thereby uncoupling autoimmunity from antitumor efficacy.

The identification of bona fide tumor-specific antigens (i.e., oncoviral antigens and neoantigens) has proven difficult in humans, and thus nonmutated self-antigens remain a commonly used target for cellular cancer immunotherapy. Indeed, T cells and antibodies recognizing nonmutated self-antigens are commonly found in patients with cancer (27–29). Nonmutated self-antigens are attractive targets, because they can be used as an “off-the-shelf” reagent for treating many cancer patients. However, since targeting self-tumor antigens requires induction of the same kind of responses that cause autoimmune diseases, whether autoimmune toxicity is an inevitable outcome of successful immunotherapy is still an issue of considerable concern to the field (30–33).

In order to address therapy-induced autoimmune toxicity, the intensity of the therapeutic approach must first be considered. We recently developed an approach using OVVs to drive expansion and tumor infiltration of preexisting antigen-specific T cells and found it to be a highly potent technique for overcoming both immune tolerance to self-antigens and the suppressive microenvironment induced by solid tumors (6, 34). The present study combined OVVs and ACT, which are clinically validated therapeutic approaches, to further enhance therapeutic efficacy. We first confirmed that ACT plus OVV as a therapeutic platform was extremely potent and able to induce complete regression of established solid tumors. For simultaneous monitoring of potential autoimmune toxicity in a vital organ, we evaluated the combination approach in the RIP-gp mouse model, in which the target antigen is expressed by both the tumor and pancreatic β cells. To our surprise, the induction of diabetes in this mouse model entirely depended on the choice of OVV vector. Both VSV and VacV were highly effective at expanding transferred T_{CM} cells recognizing the target antigen gp33, but diabetes was only coupled with tumor regression when VSV was used. Both depletion of pDCs, to reduce the production of IFN- α /- β , and blockage of IFN- α /- β signaling in β cells diminished or abrogated diabetes incidence, suggesting that undesirable toxicity is the result of excess IFN- α /- β production. This conclusion was further supported by the complete tumor regression observed in the absence of β cell destruction induced by combination treatment with ACT and VacV. In contrast to VSV, VacV has evolved diverse host immune evasion strategies by acquiring key host genes through genetic recombination. One such evasion-related captured gene product is B18R, a soluble factor that neutralizes and restricts IFN- α /- β signaling (21). Deletion of B18R from the VacV genome as well as overwhelming of B18R with pIC treatment resulted in diabetes in an IFN- α /- β -dependant manner, confirming a pathogenic role of IFN- α /- β and revealing a novel advantage inherently associated with VacV as an oncolytic immune booster.

Interestingly, and most important, we found that blocking the IFN- α /- β pathway in either case (i.e., VSV or VacV) did not compromise antitumor immunity. IFN- α /- β is a pleiotropic cytokine with a multimodal role in the promotion of innate and adaptive immune responses (35, 36). In particular, IFN- α /- β functions as a signal 3 cytokine and is critical for the priming of naive T cells. As such, many immunotherapy protocols endeavor to maximize IFN- α /- β induction in order to augment the magnitude of the antitumor responses. However, the role of IFN- α /- β in secondary T cell responses is less clear. Although many studies have proposed

that IFN- α /- β performs a similar role during a recall response (37), a recent report by Hosking and colleagues pointed out that those memory cells were intrinsically abnormal because they were generated in the absence of IFN- α /- β signaling during primary activation (i.e., using IFN- α /- β -deficient mice or receptor-deficient precursor T cells). To overcome this problem, Hosking et al. created an inducible deletion model in which the primary immune response was normal, and IFN- α /- β receptor deletion was performed only prior to secondary stimulation. They demonstrated that the recall immune response was independent of functional IFN- α /- β signaling (38). In agreement with this conclusion, our results indicate that neither the magnitude of expansion nor the antitumor functionality of adoptively transferred T_{CM} cells requires IFN- α /- β .

Finally, we demonstrated that IFN- α /- β did not influence the ability of therapy-induced T cells to access the islet but rather upregulated MHC I expression on islet cells, rendering them more susceptible to T cell killing. This conclusion is supported by evidence from both preclinical and clinical studies (24, 39). Using the same RIP-gp model, Lang and colleagues showed that highly activated gp33-specific CD8⁺ T cells could “peacefully coexist” with pancreatic β cells expressing gp33 but that concurrent induction of IFN- α /- β by systemic viral infection broke the balance and converted potential autoreactivity into overt autoimmune disease as a result of the upregulation of MHC I on β cells (24). Another study by Coppieters et al. indicated that increased HLA expression is one of the first features of islet distress, which is correlated with the presence of autoreactive CD8⁺ T cells and insulinitis in type 1 diabetes (39). Interestingly, we observed that the blockage of the IFN- α /- β pathway prevented MHC I upregulation in β cells, but this effect was not shared by cells in the tumor, suggesting that, in the absence of IFN- α /- β signaling, other inflammatory cytokines may contribute to tumor MHC I upregulation due to oncolytic viral replication.

Two additional points are worthy of consideration. First, it has been reported in 2 separate studies that infusion with T cells engineered to express a recombinant TCR targeting MAGE-A3 was associated with lethal cardiopulmonary and neurologic toxicity (10, 11). This on-target toxicity was interpreted as a failure of the recombinant TCR, which had unnaturally enhanced affinity for MAGE-A3, to distinguish between cancer cells and normal cells expressing a cross-reactive peptide (11, 40). However, all patients who died as a result of this therapy received cyclophosphamide, a lymphodepletion regimen that induces IFN- α /- β and is commonly used prior to ACT (41). Furthermore, IFN- α /- β induction by other preconditioning chemotherapeutic agents is accompanied by upregulation of MHC I (42). Therefore, our results and conclusions may offer an alternative explanation that implicates the induction of IFN- α /- β and subsequent MHC I upregulation rather than enhanced TCR affinity as the mediator of on-target, off-tumor toxicity. This hypothesis could be uniquely addressed using our combination therapy, since preconditioning was not required. Additionally, it has been proposed that deletion of viral anti-IFN- α /- β gene products (e.g., B18R in VacV) or overexpression of IFN- β would increase antitumor immunity (43–45). This proposal is well justified for oncolytic therapy-mediated activation of naive tumor-reactive T cells, however, excess production of IFN- α /- β may be deleterious when combining an OV with a more robust, tumor-reactive cell-based therapy such as ACT and/or PD-1 blockade.

In conclusion, our results demonstrate that ACT plus OVV therapy represents a synergistic combination that overcomes the various levels of regulatory mechanisms including self-tolerance and tumor suppression. Furthermore, we identified IFN α / β as a mediator that links antitumor immunity with autoimmune toxicity and found that rational choice of an OVV vector or IFN- α /- β blockade could abrogate autoimmune damage without affecting antitumor activities. We believe that our results suggest a possibility to uncouple these two clinical events even with intensified therapeutic regimens by targeting IFN- α /- β signaling. Considering that IFN- α /- β has a major effect on virtually all autoimmune diseases and that the development of IFN- α /- β blockade is currently underway (46), our findings may have broad clinical implications in the field of cancer immunotherapy.

Methods

Mice. All mice were bred and housed in the Central Animal Facility at McMaster University, a specific pathogen-free facility. RIP-gp mice [B6.Cg -Tg(Ins2-GP)34-20Olds] were a gift of Pamela Ohashi (University of Toronto, Toronto, Ontario, Canada) and were crossed with C57BL/6-Elite mice (purchased from Charles River Laboratories) to generate heterozygous mice for experimental use. 24H9 mice, a transgenic mouse strain that carries a TCR recognizing a H-2K^b-restricted epitope of DCT_{180–188} (SVYDFVWL), were a gift of Arthur Hurwitz (National Cancer Institute, Frederick, Maryland, USA). P14 mice (B6.Cg-Tcr^{tm1Mom} Tg(TcrLCMV)327Sdz), a transgenic mouse strain that carries a TCR recognizing an H-2D^b-restricted epitope of LCMV-GP_{33–41} (KAVYNFATM), were purchased from Taconic Breeding Laboratories. RIP-gp/IFNAR-KO mice were generated by crossbreeding RIP-gp heterozygosity onto a homozygous *IFNAR1*^{-/-} background (B6.129S2-*Ifnar1*^{tm1Agt}; provided by Ali Ashkar, McMaster University, Hamilton, Ontario, Canada).

Cell lines and in vitro T cell differentiation. All cells were maintained at 37 °C in a humidified atmosphere with 5% CO₂. B16F10 and B16-gp33 cells (B16F10 cells stably transfected with a minigene corresponding to the gp33 peptide) (18) were maintained in MEM/F11 containing 10% FBS, 2 mM L-glutamine, 5 ml sodium pyruvate, 5 ml nonessential amino acids, 5 ml vitamin solution, 55 μ M 2-mercaptoethanol, 100 U/ml penicillin, and 100 ng/ml streptomycin (Thermo Fisher Scientific). Bulk splenocytes from transgenic mice were isolated and cultured for 7 days in RPMI 1640 supplemented with 10% FBS, penicillin-streptomycin (100 U/ml and 100 ng/ml, respectively), L-glutamine (2 mM), and 2-mercaptoethanol (55 μ M). Splenocytes were stimulated with 100 ng/ml DCT or gp33 peptide (Biomer Technologies) in the presence of 10 ng/ml IL-15, 10 ng/ml IL-21 (BioLegend), and 20 ng/ml rapamycin (Sigma-Aldrich).

Viruses. VSV-gp33 (47) and VacV-gp33 (48) vectors are recombinant vesicular stomatitis and vaccinia viruses, respectively, that express the dominant CD8⁺ and CD4⁺ T cell epitopes of the lymphocytic choriomeningitis virus glycoprotein (LCMV-gp_{33–41} and LCMV-gp_{61–80}, respectively) in a minigene cassette. VSV-DCT is a recombinant VSV that expresses the full-length human DCT (6). VSV-GFP is a recombinant VSV that expresses GFP. VSV-gp33, VSV-DCT, and VSV-GFP were modified to abrogate their ability to inhibit IFN- α /- β responses via deletion of the methionine residue at position 51 of the matrix protein as described previously (49). VSV Δ G-gp33 was generated by insertion of the gp33 minigene into the *XhoI* and *MluI* restriction

sites of a VSV-GFP genomic plasmid lacking the glycoprotein coding sequence, using a previously described recombinant/rescue system (50). VacV Δ B18R-gp33 was generated using a synthesized DNA fragment and conventional recombination methods to bifurcate the B18R coding sequence in the VacV-gp33 genome (51).

Tumor model and combination therapy treatment. Six- to eight-week-old C57BL/6, RIP-gp, or RIP-gp/IFNAR-KO mice were challenged intradermally with 1×10^5 B16F10 or B16-gp33 cells. ACT and subsequent OVVs were administered 7 days after tumor implantation. Mice were injected i.v. with 1×10^6 T_{CM} cells in 200 μ l PBS, and 24 hours later, the indicated OVV was injected i.v. in 200 μ l PBS. VSV-gp33 and VSV Δ G-gp33 were given at 2×10^8 PFU, while VacV-gp33 and VacV Δ B18R-gp33 were given at 7.5×10^7 PFU. Tumor growth was monitored and measured with calipers. Tumor volume was calculated as the width times the length times the depth. As required, blood glucose levels were monitored using a Contour NEXT Glucometer (Ascensia Diabetes Care).

T cell purification and adoptive transfer or cytotoxicity assay. Splenocytes were extracted from mice treated with the combination therapy, and CD8⁺ T cells were isolated using an EasySep Mouse CD8⁺ T Cell Isolation Kit (STEMCELL Technologies) before rinsing and i.v. injection in 200 μ l PBS at a dose of 1×10^7 gp33-specific cells/mouse. Alternatively, purified cells were cocultured with 1×10^4 B16-gp33 cells for 18 hours at 37°C at the indicated ratios of Tetramer-positive cells to target cells (Figure 7D). T cells were removed by washing, and cell viability was quantified using a Resazurin dye assay (Sigma-Aldrich). Where indicated, cells were pretreated for 24 hours with 10^4 units/ml recombinant IFN- β (Cedarlane) (Figure 7, C and D).

Ab-mediated cell depletion and blockade. Immunodepletion studies were conducted using mAbs against CD4 (GK1.5) and CD8 (2.43), obtained from the American Type Culture Collection (ATCC). Additionally, we used a pDC depletion Ab (BX444) and an isotype control (HRPN) from Bio X Cell. Anti-CD4, anti-CD8, and the isotype control Abs (250 μ g/dose) were injected i.p. 24 hours before and after OVV injection and then twice a week thereafter until the tumor endpoint was reached. A pDC depletion Ab was given once (250 μ g), 24 hours before virus injection. To modulate IFN- α /- β sensing, RIP-gp mice were treated i.p. with an IFNARI-blocking Ab (MARI-5A3, Leinco Technologies) concurrently with tumor cell implantation and days -1, 0, and 1 (500 μ g), as well as days 3 and 5 (250 μ g) after VSV-gp33 infection. When used in conjunction with pIC, 1 mg IFNARI-blocking Ab was administered i.p. 2 hours before treatment with 200 μ g (i.p.) low-molecular-weight pIC (Sigma-Aldrich).

Cytokine quantification. Systemic cytokine levels were determined from serum samples taken before or at the indicated times (Supplemental Figure 2) after virus inoculation using a custom mouse BioPlex Express Kit (Bio-Rad). Results were read and analyzed using a MAGPIX System and MILLIPLEX Analyst 5.1 Software (Thermo Fisher Scientific), respectively. IFN- α /- β levels were measured using a LumiKine mIFN- α or LumiKine mIFN- β system (InvivoGen) according to the manufacturer's instructions and read using a SpectraMax i3 plate reader (Molecular Devices).

Flow cytometry and detection of antigen-specific T cell responses. Phycoerythrin-conjugated gp33-tetramer was purchased from the Baylor College MHC Tetramer Production Laboratory, and the following stain and Abs for flow cytometric analysis were purchased from BD Biosciences: Fc Block (catalog 553141), 7AAD (catalog 559925), Fixable Viability Stain 510 (catalog 564406), Pacific Blue Rat Anti-Mouse CD8a (clone 53-6.7), APC Rat Anti-Mouse IFN- γ (XMG1.2), PE Rat

Anti-Mouse CD4 (GK1.5), FITC Mouse Anti-Mouse H-2K^b (AF6-88.5), and APC Rat Anti-Mouse CD45 (30-F11). Samples for flow staining were single-cell suspension derived from EDTA-treated cultured cells or tissues after digestion with collagenase/DNase and mechanical disruption. Cells were treated with Fc Block and stained for surface markers followed by viability staining. For analysis of antigen-specific responses, PBMCs were extracted from blood samples using RBC lysis buffer and stimulated with DCT or gp33 peptide (1 μ g/ml) in culture at 37°C for 4 hours, and brefeldin A (GolgiPlug, BD Biosciences; 1 μ g/ml) was added for the last 3 hours of incubation. Blocking and surface staining were performed as above, and the cells were stained with fixable viability dye before fixation and permeabilization (Cytofix/Cytoperm, BD Biosciences) and intracellular staining. Data were acquired using an LSRFortessa with FACSDiva software (BD Biosciences) and analyzed with FlowJo software (Tree Star).

Immunohistochemical staining. Immunohistochemical analysis was performed on formalin-fixed, paraffin-embedded tissues using a 1:100 dilution of insulin Ab (ab181547, Abcam). Tissue sections were treated with 3% hydrogen peroxide before blocking with 5% BSA, 2% goat serum, and 0.2% Triton X-100 using the Avidin/Biotin Blocking Kit (Vector Laboratories), before probing with biotinylated anti-rabbit Ab (Vector Laboratories). Color was developed using sequential treatment with the VECTASTAIN ABC Kit (Vector Laboratories) and the ImmPACT AMEC Red Peroxidase Substrate Kit (Vector Laboratories), followed by hematoxylin counterstaining. CD8a mAb (53-6.7, BD Biosciences; 1:50 dilution) staining was performed on sections from tissues snap-frozen in Tissue-Tek OCT (Sakura), fixed with acetone and ethanol, and treated with 3% hydrogen peroxide before development using a Rat-on-Mouse HRP-Polymer Kit (Biocare Medical) and an AEC Chromogen Substrate Solution Kit (Sigma-Aldrich). MHC I mAb (27-11-13, Abcam) was diluted 1:100 in Powervision IHC Super Blocker (Leica) and preabsorbed with AffiniPure Fab Fragment Rabbit Anti-Mouse IgG and mouse serum (Jackson ImmunoResearch) before staining of frozen tissue sections on the Bond RX Automated Stainer (Leica) using a Bond Polymer Refine Red Detection System (Leica). Images were taken with Axiovert 100M microscope (ZEISS).

Statistics. GraphPad Prism for Windows (GraphPad Software) was used for graphing and statistical analyses. For all analysis, differences were considered significant at a *P* value of 0.05 or less. Differences between means were queried using an unpaired, 2-tailed Student's *t* test for individual comparisons and 1-way or 2-way ANOVA for grouped analyses with Holm-Sidak correction for multiple comparisons. The means are shown on dot plots as a horizontal black line with SD bars. Tumor endpoint (survival percentage) and diabetes endpoint (diabetes percentage) data were generated using the Kaplan-Meier method, with the tumor endpoint defined as less than 10 mm in at least 2 dimensions or greater than 20 mm in 1 dimension, and a blood sugar level above 14 mmol/l was set as the diabetes endpoint. The log-rank (Mantel-Cox) test was used for statistical analysis.

Study approval. All animal studies complied with Canadian Council on Animal Care guidelines and were approved by the Animal Research Ethics Board of McMaster University.

Author contributions

SRW performed the experiments with assistance from LC, DB, and AN. CJS, CL, and DS constructed viral vectors. JCB and JLB assisted with experimental design, data interpretation, and man-

uscript preparation. SRW and YW and conceived the project, designed the experiments, analyzed and interpreted the results, and drafted and revised the manuscript.

Acknowledgments

We thank P. Ohashi for providing the RIP-gp-transgenic mice and A. Hurwitz for providing the 24H9-transgenic mice. This work was supported by the Ontario Institute for Cancer Research, the Cana-

dian Institutes of Health Research (FRN 123516 and FRN 152954), the Canadian Cancer Society (grant 705143), and the Terry Fox Research Institute (TFRI-1073).

Address correspondence to: Yonghong Wan, Department of Pathology and Molecular Medicine, McMaster University, MDCL-5024, 1200 Main Street West, Hamilton, Ontario, Canada, L8N 3Z5. Phone: 905.525.9140; Email: wanyong@mcmaster.ca.

- Schumacher TN, Schreiber RD. Neoantigens in cancer immunotherapy. *Science*. 2015;348(6230):69–74.
- Alexandrov LB, et al. Signatures of mutational processes in human cancer. *Nature*. 2013;500(7463):415–421.
- Martin SD, et al. Low Mutation burden in ovarian cancer may limit the utility of neoantigen-targeted vaccines. *PLoS One*. 2016;11(5):e0155189.
- Morgan RA, et al. Cancer regression in patients after transfer of genetically engineered lymphocytes. *Science*. 2006;314(5796):126–129.
- Robbins PF, et al. Tumor regression in patients with metastatic synovial cell sarcoma and melanoma using genetically engineered lymphocytes reactive with NY-ESO-1. *J Clin Oncol*. 2011;29(7):917–924.
- Pol JG, et al. Maraba virus as a potent oncolytic vaccine vector. *Mol Ther*. 2014;22(2):420–429.
- Greiner JW, Zeytin H, Anver MR, Schlom J. Vaccine-based therapy directed against carcinoembryonic antigen demonstrates antitumor activity on spontaneous intestinal tumors in the absence of autoimmunity. *Cancer Res*. 2002;62(23):6944–6951.
- Schmitt TM, et al. Enhanced-affinity murine T-cell receptors for tumor/self-antigens can be safe in gene therapy despite surpassing the threshold for thymic selection. *Blood*. 2013;122(3):348–356.
- Lamers CH, et al. Treatment of metastatic renal cell carcinoma with CAIX CAR-engineered T cells: clinical evaluation and management of on-target toxicity. *Mol Ther*. 2013;21(4):904–912.
- Linette GP, et al. Cardiovascular toxicity and titin cross-reactivity of affinity-enhanced T cells in myeloma and melanoma. *Blood*. 2013;122(6):863–871.
- Morgan RA, et al. Cancer regression and neurological toxicity following anti-MAGE-A3 TCR gene therapy. *J Immunother*. 2013;36(2):133–151.
- Martin-Liberal J, Furness AJ, Joshi K, Peggs KS, Quezada SA, Larkin J. Anti-programmed cell death-1 therapy and insulin-dependent diabetes: a case report. *Cancer Immunol Immunother*. 2015;64(6):765–767.
- van den Berg JH, et al. Case Report of a Fatal serious adverse event upon administration of T cells transduced with a MART-1-specific T-cell receptor. *Mol Ther*. 2015;23(9):1541–1550.
- Klebanoff CA, et al. Central memory self/tumor-reactive CD8⁺ T cells confer superior antitumor immunity compared with effector memory T cells. *Proc Natl Acad Sci U S A*. 2005;102(27):9571–9576.
- Contreras A, et al. Enhanced local and systemic anti-melanoma CD8⁺ T cell responses after memory T cell-based adoptive immunotherapy in mice. *Cancer Immunol Immunother*. 2016;65(5):601–611.
- Bridle BW, et al. Oncolytic vesicular stomatitis virus quantitatively and qualitatively improves primary CD8⁺ T-cell responses to anticancer vaccines. *Oncoimmunology*. 2013;2(8):e26013.
- Zhu Z, et al. CD4⁺ T cell help selectively enhances high-avidity tumor antigen-specific CD8⁺ T cells. *J Immunol*. 2015;195(7):3482–3489.
- Prévost-Blondel A, Zimmermann C, Stemmer C, Kulmburg P, Rosenthal FM, Pircher H. Tumor-infiltrating lymphocytes exhibiting high ex vivo cytolytic activity fail to prevent murine melanoma tumor growth in vivo. *J Immunol*. 1998;161(5):2187–2194.
- Ohashi PS, et al. Ablation of “tolerance” and induction of diabetes by virus infection in viral antigen transgenic mice. *Cell*. 1991;65(2):305–317.
- Barchet W, Cella M, Odermatt B, Asselin-Paturel C, Colonna M, Kalinke U. Virus-induced interferon alpha production by a dendritic cell subset in the absence of feedback signaling in vivo. *J Exp Med*. 2002;195(4):507–516.
- Waibler Z, et al. Vaccinia virus-mediated inhibition of type I interferon responses is a multifactorial process involving the soluble type I interferon receptor B18 and intracellular components. *J Virol*. 2009;83(4):1563–1571.
- Manz BN, Jackson BL, Petit RS, Dustin ML, Groves J. T-cell triggering thresholds are modulated by the number of antigen within individual T-cell receptor clusters. *Proc Natl Acad Sci U S A*. 2011;108(22):9089–9094.
- Mozes E, Lovchik J, Zinger H, Singer DS. MHC class I expression regulates susceptibility to spontaneous autoimmune disease in (NZBxNZW)F1 mice. *Lupus*. 2005;14(4):308–314.
- Lang KS, et al. Toll-like receptor engagement converts T-cell autoreactivity into overt autoimmune disease. *Nat Med*. 2005;11(2):138–145.
- Russell SJ, Barber GN. Oncolytic viruses as antigen-agnostic cancer vaccines. *Cancer Cell*. 2018;33(4):599–605.
- Gujar SA, Lee PW. Oncolytic virus-mediated reversal of impaired tumor antigen presentation. *Front Oncol*. 2014;4:77.
- Houghton AN, Guevara-Patiño JA. Immune recognition of self in immunity against cancer. *J Clin Invest*. 2004;114(4):468–471.
- Sharma RA, Browning MJ. Mechanisms of the self/non-self-survey in the defense against cancer: potential for chemoprevention? *Crit Rev Oncol Hematol*. 2005;56(1):5–22.
- Gee MH, et al. Antigen identification for orphan T Cell receptors expressed on tumor-infiltrating lymphocytes. *Cell*. 2018;172(3):549–563.e16.
- Pardoll DM. Inducing autoimmune disease to treat cancer. *Proc Natl Acad Sci U S A*. 1999;96(10):5340–5342.
- Naftzger C, Takechi Y, Kohda H, Hara I, Vijayasaradhi S, Houghton AN. Immune response to a differentiation antigen induced by altered antigen: a study of tumor rejection and autoimmunity. *Proc Natl Acad Sci U S A*. 1996;93(25):14809–14814.
- Bowne WB, et al. Coupling and uncoupling of tumor immunity and autoimmunity. *J Exp Med*. 1999;190(11):1717–1722.
- Gilboa E. The risk of autoimmunity associated with tumor immunotherapy. *Nat Immunol*. 2001;2(9):789–792.
- Bridle BW, et al. Privileged Antigen Presentation in Splenic B Cell Follicles Maximizes T Cell Responses in Prime-Boost Vaccination. *J Immunol*. 2016;196(11):4587–4595.
- Kolumam GA, Thomas S, Thompson LJ, Sprent J, Murali-Krishna K. Type I interferons act directly on CD8 T cells to allow clonal expansion and memory formation in response to viral infection. *J Exp Med*. 2005;202(5):637–650.
- Keppeler SJ, Rosenits K, Koegl T, Vucikujia S, Aichele P. Signal 3 cytokines as modulators of primary immune responses during infections: the interplay of type I IFN and IL-12 in CD8 T cell responses. *PLoS One*. 2012;7(7):e40865.
- McNab F, Mayer-Barber K, Sher A, Wack A, O’Garra A. Type I interferons in infectious disease. *Nat Rev Immunol*. 2015;15(2):87–103.
- Hosking MP, Flynn CT, Whitton JL. Type I IFN Signaling Is Dispensable during Secondary Viral Infection. *PLoS Pathog*. 2016;12(8):e1005861.
- Coppieters KT, et al. Demonstration of islet-autoreactive CD8 T cells in insulinitic lesions from recent onset and long-term type 1 diabetes patients. *J Exp Med*. 2012;209(1):51–60.
- Cameron BJ, et al. Identification of a Titin-derived HLA-A1-presented peptide as a cross-reactive target for engineered MAGE A3-directed T cells. *Sci Transl Med*. 2013;5(197):197ra103.
- Schiavoni G, et al. Cyclophosphamide induces type I interferon and augments the number of CD44(hi) T lymphocytes in mice: implications for strategies of chemoimmunotherapy of cancer. *Blood*. 2000;95(6):2024–2030.
- Wan S, Pestka S, Jubin RG, Lyu YL, Tsai YC, Liu LF. Chemotherapeutics and radiation stimulate MHC class I expression through elevated interferon-beta signaling in breast cancer cells. *PLoS One*. 2012;7(3):e32542.
- Chiocca EA, Rabkin SD. Oncolytic viruses and their application to cancer immunotherapy. *Cancer Immunol Res*. 2014;2(4):295–300.
- Kirn DH, Wang Y, Le Boeuf F, Bell J, Thorne SH. Targeting of interferon-beta to produce a specific, multi-mechanistic oncolytic vaccinia virus.

- PLoS Med.* 2007;4(12):e353.
45. Willmon CL, et al. Expression of IFN-beta enhances both efficacy and safety of oncolytic vesicular stomatitis virus for therapy of mesothelioma. *Cancer Res.* 2009;69(19):7713-7720.
46. Oon S, Wilson NJ, Wicks I. Targeted therapeutics in SLE: emerging strategies to modulate the interferon pathway. *Clin Transl Immunology.* 2016;5(5):e79.
47. Zhang L, et al. Delivery of viral-vectored vaccines by B cells represents a novel strategy to accelerate CD8(+) T-cell recall responses. *Blood.* 2013;121(13):2432-2439.
48. Oldstone MB, Tishon A, Eddleston M, de la Torre JC, McKee T, Whitton JL. Vaccination to prevent persistent viral infection. *J Virol.* 1993;67(7):4372-4378.
49. Boudreau JE, et al. Recombinant vesicular stomatitis virus transduction of dendritic cells enhances their ability to prime innate and adaptive antitumor immunity. *Mol Ther.* 2009;17(8):1465-1472.
50. Roberts A, Buonocore L, Price R, Forman J, Rose JK. Attenuated vesicular stomatitis viruses as vaccine vectors. *J Virol.* 1999;73(5):3723-3732.
51. Rintoul JL, et al. A selectable and excisable marker system for the rapid creation of recombinant poxviruses. *PLoS One.* 2011;6(9):e24643.